

Synthesis of ^{18}F -Fluoroalkyl- β -D-Glucosides and Their Evaluation as Tracers for Sodium-Dependent Glucose Transporters

Tjibbe J. de Groot, PhD¹; Maike Veyhl, PhD²; Christelle Terwinghe¹; Véronique Vanden Bempt, MSc¹; Patrick Dupont, PhD¹; Luc Mortelmans, MD, PhD¹; Alfons M. Verbruggen, PhD¹; Guy M. Bormans, PhD¹; and Hermann Koepsell, MD²

¹Laboratory for Radiopharmaceutical Chemistry and Department of Nuclear Medicine, Universitaire Ziekenhuizen Gasthuisberg, Leuven, Belgium; and ²Institute of Anatomy and Cell Biology, Bayerische Julius-Maximilians-Universität, Würzburg, Germany

Three ω - ^{18}F -fluoro-*n*-alkyl- β -D-glucosides (alkyl = ethyl (**5a**), *n*-butyl (**5b**), and *n*-octyl (**5c**)) were synthesized and evaluated as potential substrates for the sodium/D-glucose cotransporter SGLT1. **Methods:** The ligands were prepared by ^{18}F -fluoride displacement of the corresponding tetraacetyl-protected tosylate alkylglucoside precursors in CH_3CN , followed by hydrolysis of the protective acetate esters with NaOMe/MeOH . Transport of the nonradioactive analogs **5a**, **5b**, and **5c** by the human sodium-D-glucose cotransporter hSGLT1 was characterized in vitro in oocytes of *Xenopus laevis* that expressed hSGLT1. The biodistribution of the tracers was determined in mice and the presence of metabolites in the blood was investigated. Compound **5a** was also evaluated in mice pretreated with phlorizin. The intrarenal distribution of **5a** in mice kidney was visualized using autoradiography. **Results:** The radiochemical yield of **5a**, **5b**, and **5c** was in the range of 8%–15% (end of bombardment) with a total synthesis time of 90 min. The in vitro evaluation after expression of the hSGLT1 showed that 2'-fluoroethyl- β -D-glucoside (**5a**) was transported with similar Michaelis-Menten K_m and V_{max} (maximum velocity) values as compared with methyl- α -D-glucopyranoside (α MDG). The more lipophilic compounds **5b** and **5c** were not transported but inhibited transport of α MDG. In vivo tissue distribution in mice revealed that **5a**, **5b**, and **5c** were cleared mainly by the renal pathway and that **5a** showed a significantly higher accumulation in the kidneys and a slower renal excretion as compared with **5b** and **5c**. Compound **5a** was retained mainly in the renal outer medulla containing S3 segments of proximal tubules and the accumulation could be blocked by phlorizin pretreatment. Compound **5c** passed the blood-brain barrier to some extent. **Conclusion:** The data indicate that 2'- ^{18}F -fluoroethyl- β -D-glucoside (**5a**) is a specific tracer of Na^+ -dependent glucose transport that may be used to visualize this transport activity in the S3 segments of renal proximal tubules.

Key Words: Na^+ -dependent glucose transporter; ^{18}F ; glucose; sodium/D-glucose cotransporter

J Nucl Med 2003; 44:1973–1981

Secondary active D-glucose transporters (SGLTs) play a pivotal role in the absorption of D-glucose in small intestine and in the reabsorption of D-glucose in renal proximal tubules (1,2). Up to 6 isoforms of SGLT (SGLT1–SGLT6) have been identified that differ in tissue distribution and functional properties and exhibit some species differences (1–3). SGLT1 is expressed in the luminal membrane of small intestinal enterocytes, where it is responsible for the absorption of D-glucose, and in the S3 segment of renal proximal tubules, where it mediates high-affinity reabsorption of D-glucose that has not been reabsorbed earlier. SGLT2 is a low-affinity sodium-D-glucose cotransporter that is expressed in the S1 and S2 segments of renal proximal tubules and reabsorbs the bulk of ultrafiltered D-glucose (2). SGLT3 from pig has been identified as a sodium-D-glucose cotransporter that is expressed in small intestine but not in kidney (3,4); however, no transport function could be detected for human SGLT3 (5). Transcription of SGLT1 has also been observed in several tumor cell lines and various human carcinomas (6,7).

The SGLT transporters exhibit a variety of important physiologic functions and are of biomedical importance. Genetic defects of the SGLT1 and SGLT2 result in glucose-galactose malabsorption (8) or familial renal glycosuria (9), respectively. In a rat model of short bowel syndrome, uptake of galactose could be enhanced by transfection of SGLT-1 into colon mucosa (10). Compounds that inhibit SGLTs are currently explored for the treatment of noninsulin-dependent diabetes mellitus with the aim of increasing the urinary excretion of excess plasma glucose (11). The decrease of methyl- α -D-glucopyranoside (α MDG) uptake in isolated proximal tubules correlates with nephrotoxicity of xenobiotics (12).

Recently it has been shown that SGLT1 is also expressed in neurons of the central nervous system (CNS) and in endothelial cells of brain arteries and capillaries (13,14; H. Koepsell, unpublished data, 2003). This was a surprising observation since it is generally believed that transport of

Received Apr. 4, 2003; revision accepted Aug. 28, 2003.
For correspondence or reprints contact: Tjibbe de Groot, PhD, Laboratory of Radiopharmaceutical Chemistry and Radiopharmacy, Universitaire Ziekenhuizen Gasthuisberg, Herestraat 49, B-3000 Leuven, Belgium.
E-mail: tjibbe.degroot@uz.kuleuven.ac.be

D-glucose in the CNS is only mediated by facilitated diffusion through GLUT1 and GLUT3 transporters. It has been established that GLUT1 facilitates transport of glucose over the blood–brain barrier (BBB) and that GLUT3 mediates transport of glucose into neurons (15,16). The functional role of SGLT1 in brain is not well understood. Poppe et al. (13) raised the hypothesis that SGLT1 may account for the increased availability of glucose during metabolic stress in the brain. They found a local accumulation of ^{14}C - αMDG after inducing a seizure in rat brain. They argued that the increased uptake of αMDG may reflect the induction of SGLT1 by the increased demand for D-glucose, since αMDG is a substrate of SGLT1 but not of GLUT1 and GLUT3 (17).

Given the fact that 2-deoxy-D-glucose is a poor substrate for SGLT1 (18), PET studies with ^{18}F -FDG do not allow evaluation of the function of SGLT1 in brain or other tissues. The aim of this study was to prepare an ^{18}F -labeled substrate with high affinity for SGLT1 that would allow studying the function of the SGLT1 transporter with PET in vivo. Glucosides with an alkyl moiety in the β -position appeared to be appropriate starting compounds, as it has been reported that they have a higher affinity for SGLT1 compared with D-glucose (19). Some of these compounds were found to inhibit uptake of D-glucose but are not transported themselves. This may be due to the longer alkyl side chain that increases the affinity for SGLT1 but prevents the translocation step (19).

In this study, we describe the synthesis and evaluation of 2'- ^{18}F -fluoroethyl- β -D-glucoside (**5a**), ω - ^{18}F -fluoro-*n*-butyl- β -D-glucoside (**5b**), and ω - ^{18}F -fluoro-*n*-octyl- β -D-glucoside (**5c**). The corresponding nonradioactive compounds **5a**, **5b**, and **5c** were also prepared. In vitro, **5a**, **5b**, and **5c** were evaluated for their ability to be transported by human SGLT1 (hSGLT1) and for their inhibition of transport of αMDG by hSGLT1. The biologic behavior of **5a**, **5b**, and **5c** in vivo was determined in mice.

MATERIALS AND METHODS

Acetobromoglucose (**1**) was obtained from Sigma. β -Bromoethyl-2,3,4,6-tetra-*O*-acetyl- β -D-glucoside was prepared as described by Dahmén et al. (20). ^1H and ^{13}C NMR spectra were recorded on a Gemini 200-MHz spectrometer (Varian). Chemical shifts are reported in parts per million relative to tetramethylsilane ($\delta = 0$). Exact mass measurements were performed on a time-of-flight spectrometer (LCT; Micromass) equipped with a standard electrospray ionization (ESI) interface. Samples were infused in 2-propanol/water (1:1 v/v) with a Harvard 22 syringe pump (Harvard Instruments). For accurate mass calculations, a lock mass solution of 0.1 mg/mL solution of Kryptofix 2.2.2. (Merck) at a flow rate of 1 $\mu\text{L}/\text{min}$ was coinfused. Preparative column chromatography was performed on silica gel 60 (Merck). Batches of ^{18}F -fluoride were prepared by an $^{18}\text{O}(\text{p},\text{n})^{18}\text{F}$ reaction by irradiation of 2 mL ^{18}O -enriched water (Cortec) in a titanium target with 10-MeV protons using a Cyclone 10/5 cyclotron (IBA). Quality control of labeled **3a**, **3b**, and **3c** was performed on a Carbohydrate Amino column (10 μm , 4.1×300 mm; Alltech), eluted with a

linear gradient of H_2O , CH_3CN , and 0.1 mol/L NaF. The gradient was composed as follows (v/v/v): 0 min, 10:90:0; 6 min, 0:50:50; 7.5 min, 0:0:100. The column effluent was monitored with a refractive index detector, an ultraviolet detector set at 254 nm, and a 2-in. (5.1 cm) NaI(Tl) scintillation detector coupled to a single-channel analyzer. Output of the detectors was analyzed by a RaChel analysis program (Lablogig). Radiochemical yields were corrected for decay. The identity of the ^{18}F -labeled compounds was confirmed on high-performance liquid chromatography (HPLC) by coelution of authentic material.

Synthesis

2'-Tosyloxyethyl-2,3,4,6-Tetra-*O*-Acetyl- β -D-Glucoside (3a). A solution of 0.49 g (1.1 mmol) 2'-bromoethyl-2,3,4,6-tetra-*O*-acetyl- β -D-glucoside (**20**) and 0.60 g (2.1 mmol) silver tosylate in 25 mL CH_3CN was refluxed for 5 d shielded from light. The solvent was evaporated and the residue was applied on a silica column eluted with a gradient of ether/hexane (1:1 v/v increased to 2:1 v/v). Yield was 0.37 g (0.7 mmol, 63%) of a white solid. ^1H NMR (CDCl_3) δ 2.00, 2.02, 2.05, 2.08 ($4 \times \text{s}$, 12H), 2.46 (s, 3H), 3.68 (m, 1H), 3.90 (dm, 2H), 4.10 (dd, 1H), 4.15 (t, 2H), 4.24 (dd, 1H), 4.51 (d, 1H, $^3J = 7.8$ Hz), 4.95 (dd, 1H), 5.04 (t, 1H), 5.19 (t, 1H), 7.37 (d, 2H), 7.78 (d, 2H).

2'-Fluoroethyl-2,3,4,6-Tetra-*O*-Acetyl- β -D-Glucoside (4a). To a solution of 3.9 g (10 mmol) 1,2,3,4,6-penta-*O*-acetyl- β -D-glucose and 0.8 mL (13.6 mmol) 2-fluoroethanol in 20 mL CH_2Cl_2 at 0°C was added 6.2 mL (50 mmol) boron trifluoride etherate. The mixture was stirred overnight at room temperature. The reaction mixture was poured onto ice and neutralized with saturated NaHCO_3 solution. The water layer was extracted with CH_2Cl_2 and the organic layer was dried over MgSO_4 . Purification was performed on a silica column eluted with ether/hexane (1:1 v/v). The desired product was allowed to crystallize from the eluent, yielding 1.3 g (3.3 mmol, 33%) of a white crystalline product. ^1H NMR (CDCl_3) δ 2.01, 2.03, 2.05, 2.09 ($4 \times \text{s}$, 12H), 3.72 (m, 1H), 3.87 (dm, 2H), 4.15 (dd, 1H), 4.28 (dd, 1H), 4.54 (dt, 2H, $^2J_{\text{HF}} = 47.6$ Hz), 4.60 (d, 1H, $^3J = 8.0$ Hz), 5.04 (dd, 1H), 5.14 (t, 1H), 5.23 (t, 1H). ^{13}C NMR (CDCl_3) δ 20.46, 61.79, 68.28, 68.74 (d, $^2J_{\text{CF}} = 21.4$ Hz), 71.08, 71.87, 72.63, 82.45 (d, $^1J_{\text{CF}} = 169.4$ Hz), 100.98, 169.47.

2'-Fluoroethyl- β -D-Glucoside (5a). To a solution of 1.3 g (3.3 mmol) 2'-fluoroethyl-2,3,4,6-tetra-*O*-acetyl- β -D-glucoside (**4a**) in 25 mL methanol was added 5 mL of a solution of 100 mg sodium in 20 mL methanol and stirring was continued for 30 min. An amount of 2 g silica was added and the solvent was evaporated. The silica impregnated with the crude product was applied on a silica column that was eluted with acetonitrile, yielding 0.6 g (2.6 mmol, 80%) of a colorless oil. ^1H NMR (CD_3OD) δ 3.1–3.4 (m, 4H), 3.6–4.2 (m, 4H), 4.32 (d, 1H, $^3J = 7.4$ Hz), 4.59 (dt, 2H, $^2J_{\text{HF}} = 47.6$ Hz). ^{13}C NMR (CD_3OD) δ 62.60, 68.13 (d, $^2J_{\text{CF}} = 18.3$ Hz), 70.34, 73.65, 76.99, 77.17, 83.40 (d, $^1J_{\text{CF}} = 164.8$ Hz), 103.21. Exact mass (ESI-MS) for $\text{C}_8\text{H}_{15}\text{FO}_6$ [$\text{M}+\text{Na}$] $^+$: found 249.0754, calculated 249.0750.

ω -Hydroxy-*n*-Butyl-2,3,4,6-Tetra-*O*-Acetyl- β -D-Glucoside (2b). An amount of 5 mL (56 mmol) 1,4-butanediol was added to 200 mL CH_2Cl_2 , followed by a sufficient amount (10 mL) of dioxane to result in a homogeneous solution. Next, 1.8 g (8.3 mmol) yellow HgO , 0.14 g (0.39 mmol) HgBr_2 , and 6 g MgSO_4 were added and, after stirring for 15 min, 4.2 g (10.2 mmol) 2,3,4,6-tetra-*O*-acetyl- α -D-glucopyranosyl bromide (**1**) was added in one portion. The flask was shielded from light and stirring was continued overnight.

The suspension was filtered over celite, and the filtrate was concentrated in vacuo and applied on a silica column eluted with a gradient of ethyl acetate/hexane (1:2 v/v increased to 1:1 v/v). Yield was 3.7 g (8.7 mmol, 85%) of a colorless oil. ^1H NMR (CDCl_3) δ 1.65 (m, 4H), 2.00, 2.03, 2.05, 2.09 (4 \times s, 12H), 3.55 (dt, 1H), 3.63 (t, 2H), 3.72 (m, 1H), 3.93 (dt, 1H), 4.14 (dd, 1H), 4.27 (dd, 1H), 4.53 (d, 1H, $^3J = 7.8$ Hz), 4.98 (dd, 1H), 5.08 (t, 1H), 5.22 (t, 1H). ^{13}C NMR (CDCl_3) δ 20.36, 25.65, 29.02, 61.76, 62.01, 68.29, 69.81, 71.17, 71.60, 72.66, 100.64, 169.44, 169.45, 170.32, 170.75.

ω -Tosyloxy-*n*-Butyl-2,3,4,6-Tetra-*O*-Acetyl- β -*D*-Glucoside (3b). To a solution of 3.2 g (8.1 mmol) ω -hydroxy-*n*-butyl-2,3,4,6-tetra-*O*-acetyl- β -*D*-glucoside (**2b**) and 5 mL (35 mmol) triethylamine in 100 mL CH_2Cl_2 at 0°C was added 3.1 g (16.3 mmol) *p*-toluenesulfonyl chloride. After stirring the solution overnight at room temperature, the solution was extracted twice with water. The solution was dried over MgSO_4 and concentrated in vacuo, and the residual oil was applied on a silica column eluted with hexane/ethyl acetate (2:1 v/v). Yield was 1.6 g (2.9 mmol, 36%) of an oil that solidified on standing. ^1H NMR (CDCl_3) δ 1.65 (m, 4H), 2.00, 2.02, 2.05, 2.08 (4 \times s, 12H), 2.46 (s, 3H), 3.48 (dt, 1H), 3.68 (m, 1H), 3.85 (dt, 1H), 4.03 (t, 2H), 4.12 (dd, 1H), 4.26 (dd, 1H), 4.46 (d, 1H, $^3J = 7.6$ Hz), 4.96 (dd, 1H), 5.02 (t, 1H), 5.19 (t, 1H), 7.36 (d, 2H), 7.79 (d, 2H). ^{13}C NMR (CDCl_3) δ 20.48, 21.52, 25.34, 61.86, 68.35, 68.86, 70.05, 71.23, 71.49, 72.78, 100.70, 127.89, 129.90, 132.70, 144.65, 169.53, 170.38

ω -Fluoro-*n*-Butyl-2,3,4,6-Tetra-*O*-Acetyl- β -*D*-Glucoside (4b). An amount of 6.7 g (16.4 mmol) ω -hydroxy-*n*-butyl 2,3,4,6-tetra-*O*-acetyl- β -*D*-glucoside (**2b**) was dissolved in 320 mL CH_2Cl_2 containing 2.6 mL (32 mmol) pyridine and cooled to 0°C . To this solution was added 2.3 mL (18.2 mmol) diethylaminosulfur trifluoride (DAST) dissolved in 20 mL CH_2Cl_2 and stirring was continued at the same temperature for 20 min. The solution was poured into 400 mL saturated NaHCO_3 solution at 0°C , and the organic layer was separated and washed twice with 100 mL water. After drying over MgSO_4 , the solution was evaporated and the residue was applied on a silica column eluted with hexane/ethyl acetate (3/1 v/v), yielding 1.1 g (2.6 mmol, 16%) of a white solid. ^1H NMR (CDCl_3) δ 1.70 (m, 4H), 2.01, 2.02, 2.04, 2.09 (4 \times s, 12H), 3.54 (dt, 1H), 3.70 (m, 1H), 3.92 (dt, 1H), 4.14 (dd, 1H), 4.25 (dd, 1H), 4.45 (dt, 2H, $^2J_{\text{HF}} = 48.0$ Hz), 4.51 (d, 1H, $^3J = 7.8$ Hz), 4.99 (dd, 1H), 5.08 (t, 1H), 5.21 (t, 1H).

ω -Fluoro-*n*-Butyl- β -*D*-Glucoside (5b). The same procedure for the hydrolysis was used as described for 2'-fluoroethyl- β -*D*-glucoside (**5a**). Yield was 0.5 g (1.4 mmol, 53%) of a colorless oil. ^1H NMR (CD_3OD) δ 1.6–1.9 (m, 4H), 3.1–3.4 (m, 4H), 3.5–3.7 (m, 2H), 3.8–4.0 (m, 2H), 4.27 (d, 1H, $^3J = 7.6$ Hz), 4.45 (dt, 2H, $^2J_{\text{HF}} = 48.0$ Hz). ^{13}C NMR (CD_3OD) δ 26.57, 28.16, 62.72, 70.18, 71.58, 75.04, 77.83, 78.0, 84.78 ($^1J_{\text{CF}} = 164.8$ Hz), 104.30. Exact mass (ESI-MS) for $\text{C}_{10}\text{H}_{19}\text{FO}_6$ [$\text{M}+\text{Na}$] $^+$: found 277.1068, calculated 277.1063.

ω -Hydroxy-*n*-Octyl-2,3,4,6-Tetra-*O*-Acetyl- β -*D*-Glucoside (2c). The title compound was prepared from 1,8-octanediol as described for ω -hydroxy-*n*-butyl-2,3,4,6-tetra-*O*-acetyl- β -*D*-glucoside (**2b**) (addition of dioxane was not required). Yield was 3.9 g (8.6 mmol, 84%) of a crystallized oil. ^1H NMR (CDCl_3) δ 1.30 (m, 8H), 1.56 (m, 4H), 2.01, 2.03, 2.04, 2.09 (4 \times s, 12H), 3.48 (dt, 1H), 3.60 (t, 2H), 3.70 (m, 1H), 3.87 (dt, 1H), 4.13 (dd, 1H), 4.27 (dd, 1H), 4.50 (d, 1H, $^3J = 7.6$ Hz), 4.97 (dd, 1H), 5.07 (t, 1H), 5.20 (t, 1H). ^{13}C NMR (CDCl_3) δ 20.27, 20.40, 25.40, 28.92, 29.05, 32.38, 61.76,

62.43, 68.26, 69.90, 71.14, 71.45, 72.66, 100.58, 169.23, 169.36, 170.20, 170.63.

ω -Tosyloxy-*n*-Octyl-2,3,4,6-Tetra-*O*-Acetyl- β -*D*-Glucoside (3c). The same procedure was used as described for ω -tosyloxy-*n*-butyl-2,3,4,6-tetra-*O*-acetyl- β -*D*-glucoside (**3b**). Yield was 0.93 g (1.5 mmol, 36%) of a colorless oil that solidified on standing. ^1H NMR (CDCl_3) δ 1.3 (m, 8H), 1.5 (m, 4H), 2.01, 2.03, 2.04, 2.09 (4 \times s, 12H), 2.46 (s, 3H), 3.47 (dt, 1H), 3.70 (m, 1H), 3.86 (dt, 1H), 4.02 (t, 2H), 4.14 (dd, 1H), 4.28 (dd, 1H), 4.50 (d, 1H, $^3J = 7.6$ Hz), 4.98 (dd, 1H), 5.08 (t, 1H), 5.21 (t, 1H), 7.36 (d, 2H), 7.79 (d, 2H). ^{13}C NMR (CDCl_3) δ 20.42, 21.42–29.14, 61.85, 68.38, 70.02, 70.50, 71.23, 71.60, 72.75, 100.73, 127.80, 129.78, 132.70, 144.65, 169.30, 169.45, 170.30, 170.69.

ω -Fluoro-*n*-Octyl-2,3,4,6-Tetra-*O*-Acetyl- β -*D*-Glucoside (4c). The title compound was prepared as described for ω -fluoro-*n*-butyl-2,3,4,6-tetra-*O*-acetyl- β -*D*-glucoside (**4b**). Yield was 1.4 g (3.1 mmol, 30%) of a white solid. ^1H NMR (CDCl_3) δ 1.3–1.8 (m, 12H), 2.01, 2.03, 2.04, 2.09 (4 \times s, 12H), 3.49 (dt, 1H), 3.69 (m, 1H), 3.87 (dt, 1H), 4.13 (dd, 1H), 4.29 (dd, 1H), 4.44 (dt, 2H, $^2J_{\text{HF}} = 47.4$ Hz), 4.50 (d, 1H, $^3J = 7.6$ Hz), 4.99 (dd, 1H), 5.08 (t, 1H), 5.21 (t, 1H). ^{13}C NMR (CDCl_3) δ 20.27, 24.80–32.32, 61.79, 68.29, 69.93, 71.17, 71.53, 72.66, 83.92 ($^1J_{\text{CF}} = 164.8$ Hz), 100.64, 169.17, 169.36, 170.20, 170.60.

ω -Fluoro-*n*-Octyl- β -*D*-Glucoside (5c). The title compound was prepared as described for ω -fluoro-*n*-butyl- β -*D*-glucoside (**5b**). Yield was 0.5 g (1.6 mmol, 52%) of a white solid. ^1H NMR (CD_3OD) δ 1.3–1.8 (m, 12H), 3.1–3.4 (m, 4H), 3.53 (dt, 1H), 3.66 (dd, 1H), 3.86 (dd, 1H), 3.93 (t, 1H), 4.24 (d, 1H, $^3J = 7.8$ Hz), 4.40 (dt, 2H, $^2J_{\text{HF}} = 47.6$ Hz). ^{13}C NMR (CD_3OD) δ 26.93, 30.27–31.70, 62.75, 70.85, 71.64, 75.10, 77.89, 78.13, 84.89 ($^1J_{\text{CF}} = 163.2$ Hz), 104.39. Exact mass (ESI-MS) for $\text{C}_{14}\text{H}_{27}\text{FO}_6$ [$\text{M}+\text{H}$] $^+$: found 311.1882, calculated 311.1869.

2'- ^{18}F -Fluoroethyl- β -*D*-Glucoside (5a). After cyclotron irradiation, the content of the ^{18}F -fluoride-target was passed over a disposable anion-exchange column (Accell plus QMA; Waters) to trap ^{18}F -fluoride. The column was eluted with a solution of 18 mg Kryptofix 2.2.2. and 1.6 mg K_2CO_3 in 0.75 mL $\text{CH}_3\text{CN}/\text{H}_2\text{O}$ (95:5 v/v) and the eluate was dried by 2 consecutive evaporations with 0.3 mL CH_3CN . A solution of 5 mg 2'-tosyloxyethyl-2,3,4,6-tetra-*O*-acetyl- β -*D*-glucoside (**3a**) in 0.5 mL CH_3CN was added to 5,000 MBq Kryptofix/ K_2CO_3 / ^{18}F -fluoride and the mixture was heated in a closed vial at 60°C during 20 min. The mixture was cooled, eluted over a silica Sep-Pak column (Waters) with 5 mL ether, and concentrated, yielding 630 MBq (17%, 40 min) of the crude tetraacetate. Preparative HPLC was performed on a μ Bondapak column (7.8 \times 300 mm; Waters), eluted with $\text{CH}_3\text{CN}/\text{H}_2\text{O}$ 45:55 (v/v) at 4 mL/min (retention time [t_{R}] = 7 min 50 s). After dilution of the effluent to 10% CH_3CN in H_2O , the solution was applied on a C_{18} light Sep-Pak column (Waters). The tetraacetate was eluted from the Sep-Pak with 2 mL methanol and, after addition of 0.2 mL of a 0.22 mol/L solution of $\text{NaOCH}_3/\text{CH}_3\text{OH}$, the mixture was stirred at room temperature for 30 min. The solution was applied on a silica Sep-Pak followed by 3 mL CH_3CN and the solvent was evaporated. The residue was dissolved in 0.9% NaCl solution, yielding 220 MBq (87%, 50 min) 2'- ^{18}F -fluoroethyl- β -*D*-glucoside (**5a**). On average, the total synthesis time was 90 min and the overall decay-corrected yield was $11\% \pm 3\%$ ($n = 4$). The radiochemical purity of **5a** was assessed by HPLC on a Carbohydrate Amino column and was consistently found to be $>95\%$ ($t_{\text{R}} = 6$ min 15 s).

ω -¹⁸F-Fluoro-*n*-Butyl- β -D-Glucoside (**5b**). The title compound was prepared and analyzed as described for **5a**, except for the purification of the final product that was performed on a C₁₈ column (Hypersil BDS C₁₈ = 5 μ m; Alltech) eluted with a mixture of CH₃CN/H₂O (5:95 v/v, 1 mL/min). Compound **5b** eluted after 5 min 30 s; the radiochemical yield was 10% \pm 5% (n = 5). The radiochemical purity of **5b** was determined on a Carbohydrate Amino column and was consistently found to be >95% (t_R = 4 min 20 s).

ω -¹⁸F-Fluoro-*n*-Octyl- β -D-Glucoside (**5c**). The same procedure was applied as described for **5b**. The final product was purified on a C₁₈ column eluted with the following gradient (CH₃CN/H₂O v/v, 1 mL/min): 0–7 min 25:75; 10 min 80:20; 30 min 90:10. Compound **5c** eluted after 12 min. The radiochemical yield was 9% \pm 5% (n = 5). The radiochemical purity of **5c** was determined on a Carbohydrate Amino column and was consistently found to be >95% (t_R = 2 min 5 s).

Evaluation for Interaction with hSGLT1

Sense complementary RNA (cRNA) of hSGLT1 was synthesized as described previously (6). For expression, defolliculated *Xenopus laevis* oocytes were injected with 50 nL water containing 10 ng of hSGLT1 cRNA per oocyte. The oocytes were incubated for 3 d at 19°C in Ori buffer (5 mmol/L HEPES-Tris, pH 7.4, 100 mmol/L NaCl, 3 mmol/L KCl, 2 mmol/L CaCl₂, and 1 mmol/L MgCl₂) containing 50 mg/L gentamycin.

For tracer flux measurements, *Xenopus* oocytes were incubated for 1 h at room temperature with Ori buffer containing 10 μ mol/L ¹⁴C- α MDG (11.25 GBq/mmol; Amersham Pharmacia Biotech) plus different concentrations of either 2'-fluoroethyl- β -D-glucoside (**5a**), ω -fluoro-*n*-butyl- β -D-glucoside (**5b**), or ω -fluoro-*n*-octyl- β -D-glucoside (**5c**). The incubation was performed in the absence or presence of 100 μ mol/L phlorizin. Then the oocytes were washed and analyzed for radioactivity (6). The uptake of ¹⁴C- α MDG was calculated as the difference of its uptake in 7–10 oocytes in the absence and presence of phlorizin.

Electrical measurements of glycoside transport by hSGLT1 were performed using the 2-microelectrode voltage-clamp technique as described previously (6). Oocytes clamped at –50 mV were continuously superfused at room temperature (~3 mL/min) with Ori buffer, and inward currents that were induced by addition of different concentrations of glycosides were measured. The measurements were performed with at least 4 different oocytes from 2 different batches of oocytes.

The maximal currents that are induced by α MDG and **5a** were determined in 5 oocytes expressing hSGLT1 that were clamped at –50 mV. These oocytes were superfused respectively with Ori buffer, with Ori buffer containing 5 mmol/L α MDG, again with Ori buffer, and finally with Ori buffer containing 5 mmol/L **5a**.

Biodistribution in Mice

Animal studies were performed according to the Belgian code of practice for the care and use of animals. The solution of the ¹⁸F-labeled sugars were diluted with normal saline to a concentration of 4 MBq/mL. Male NMRI mice (body mass, 25–30 g) were sedated by intramuscular injection of 0.05 mL of a 1:4 diluted solution of Hypnorm (Duphar). Then, 0.1 mL of the tracer solution was injected in each of the mice (n = 5 at each time point) via a tail vein. The mice were killed by decapitation at 10 or 30 min after injection. Five mice were pretreated with an intraperitoneal dose of 800 mg/kg body mass phlorizin (200 mg/mL solution in 1,3-propanediol/water 60:40 v/v) 2 h before injection with **5a** and

killed after 30 min. Blood was collected in tared tubes and weighed. All organs and other body parts were dissected and their ¹⁸F radioactivity was determined in a Wizard γ -counter (Wallac). Corrections were made for background radiation and physical decay during counting. For calculation of total blood activity, blood mass was assumed to be 7% of body weight.

In Vivo Metabolism

An amount of 2 MBq **5a**, **5b**, or **5c** was injected in each of 3 mice via a tail vein. The animals were decapitated after 30 min and blood and urine were collected. The hematocrit value was determined in duplicate. The blood samples were weighed and their radioactivity was counted in a γ -sample changer. After centrifugation, plasma was collected, weighed, and diluted with 3 parts of acetonitrile. After filtration through a 0.22- μ m filter, the sample was applied on HPLC and 1.5-mL fractions were collected and their radioactivity was counted in a γ -sample changer. The residual radioactivity in the plasma pellet and the filter was also determined. The urine samples were treated and analyzed on HPLC as described for the plasma samples. To compare the uptake of **5a**, **5b**, and **5c** in red blood cells, an ANOVA with a Tukey honest significant difference post hoc test was used.

Autoradiography

To determine the in vivo intrarenal distribution, 0.1 mL of a saline solution containing 6 MBq 2'-¹⁸F-fluoroethyl- β -D-glucoside (**5a**) was injected intravenously in a sedated NMRI mouse. The animal was killed by decapitation at 30 min after injection and a kidney was rapidly removed and immediately frozen in 2-methylbutane (cooled to –25°C with liquid nitrogen). Serial frozen sections of 25 μ m were cut and mounted on microscope slides. The sections were immediately air dried at 50°C and exposed overnight to a high-performance storage phosphor screen (Packard) that was scanned in a Phosphor Imager Scanner (Packard Cyclone). Later, the sections were fixed by 20 min incubation with 4% (w/v) paraformaldehyde dissolved in phosphate-buffered saline, stained with hematoxylin, and examined by light microscopy.

RESULTS

Chemistry

2-Bromoethylglucoside was prepared as described by Dahmén et al. (20) and converted to the corresponding tosylate **3a** with silver tosylate in CH₃CN. The precursors for the synthesis of ¹⁸F-fluorobutyl- (**5b**) and ¹⁸F-fluorooctylglucoside (**5c**) were prepared using Koenigs–Knorr reaction conditions followed by tosylation of the ω -alcohol function (overall yield, 30%; Fig. 1). The Koenigs–Knorr synthesis is applied widely for the synthesis of alkyl glycosides using silver or mercury salts as catalyst (21). We found the best results with mercury(II)bromide as catalyst (22). The synthesis of the butyl derivative (**2b**) required the addition of a small amount of 1,4-dioxane to the reaction mixture to prevent separation of the 2 phases and inactivation of the mercury catalyst. Under these conditions, the β -isomers were isolated in good yields. The fluoro-derivatives **5b** and **5c** were prepared by reaction of DAST on the corresponding alcohols. To prevent hydrolysis of the 1-acetal, 2 equivalents of pyridine were added to the reaction mixture. The labeling reactions with ¹⁸F were performed

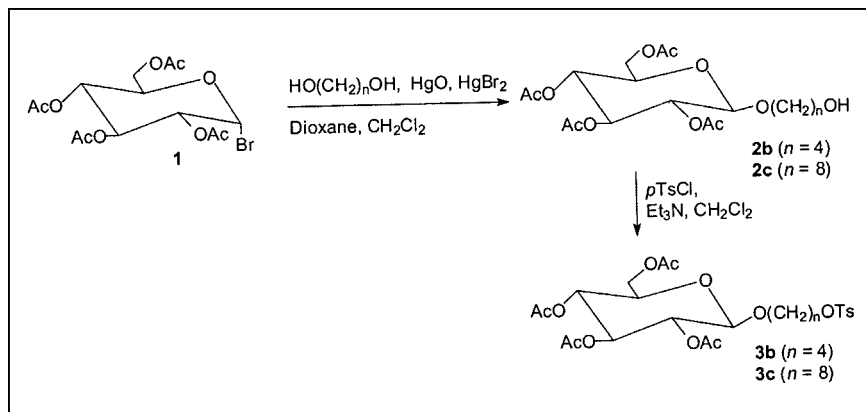


FIGURE 1. Synthesis of precursors for synthesis of ω - ^{18}F -fluoro-*n*-butyl- β -D-glucoside (**5b**) and ω - ^{18}F -fluoro-*n*-octyl- β -D-glucoside (**5c**).

using standard conditions with Kryptofix/ K_2CO_3 / ^{18}F -fluoride in CH_3CN at 60°C (Fig. 2). Hydrolysis of the protective acetate groups was performed with NaOMe/MeOH at 20°C . Hydrolysis of the 1-acetal was not found using the basic conditions, although it could be hydrolyzed under acidic conditions (1N HCl , 130°C , 10 min). The purity and identity of the final products were assessed on HPLC before injection in mice. In each case, the radiochemical purity was $>95\%$. The specific activity at the end of synthesis was estimated to be $>15 \text{ GBq}/\mu\text{mol}$. Nonradioactive impurities as determined with mass spectrometry were virtually absent ($<10 \text{ nmol}$).

Uptake Measurements with hSGLT1 Expressed in *Xenopus* Oocytes

To characterize the interactions of 2'-fluoroethyl- β -D-glucoside (**5a**), ω -fluoro-*n*-butyl- β -D-glucoside (**5b**), and ω -fluoro-*n*-octyl- β -D-glucoside (**5c**) with SGLT1, the human transporter hSGLT1 was expressed in *Xenopus* oocytes. The inhibition of expressed ^{14}C - αMDG uptake by these compounds and the currents that were induced by **5a**, **5b**, or **5c** were determined using the 2-electrode voltage-clamp technique. The measurements were performed with hSGLT1 since species differences between SGLT transporters have been described and we wanted to make sure that the obtained data are relevant for the human. In Figure 3, we tested whether the phlorizin-inhibitable uptake of ^{14}C - αMDG in hSGLT1-expressing oocytes was inhibited by different concentrations of **5a**, **5b**, or **5c**. All 3 compounds were able to inhibit αMDG uptake by hSGLT1. Fitting the Michaelis–Menten equation to the data, K_i values of $1.51 \pm 0.23 \text{ mmol/L}$ (**5a**), $1.60 \pm 0.20 \text{ mmol/L}$ (**5b**), and $66 \pm 2.9 \mu\text{mol/L}$ (**5c**) were found. In Figure 4, we determined

whether **5a**, **5b**, and **5c** were transported by hSGLT1. When *Xenopus* oocytes expressing hSGLT1 clamped at -50 mV were superfused with 5 mmol/L of αMDG , **5a**, **5b**, or **5c**, inward currents were induced by αMDG (**23**) and **5a** but not by **5b** and **5c**. This indicates that hSGLT1 mediates cotransport of Na^+ and **5a** (as has been described for D-glucose as well as αMDG), whereas **5b** and **5c** are nontransported inhibitors. To determine the maximal currents that are induced by αMDG and **5a**, 5 oocytes expressing hSGLT1 that were clamped at -50 mV were examined. The inward currents induced by αMDG and **5a** were $52.5 \pm 3.0 \text{ nA}$ and $45 \pm 4.0 \text{ nA}$ ($P < 0.05$ for difference), respectively. This indicates that the maximal transport rate of hSGLT1 for **5a** is slightly lower than that of αMDG . In Figure 5, we measured the substrate dependence of inward currents in hSGLT1-expressing *Xenopus* oocytes clamped at -50 mV that could be induced by **5a**. Fitting the Michaelis–Menten equation to the data, a K_m value of $2.6 \pm 0.2 \text{ mmol/L}$ was obtained. This value is in the same range as the apparent K_i value determined for the inhibition of αMDG uptake by **5a**.

In Vivo Evaluation

The results of the tissue distribution study in mice are shown in Table 1. All 3 ^{18}F -fluoroalkyl glucosides were cleared mainly by the kidneys. Interestingly, the excretion of **5b** and **5c** into the urine was more rapid compared with the shorter-chain 2'- ^{18}F -fluoroethyl- β -D-glucoside **5a**.

To study the intrarenal distribution of **5a** in more detail, slices of a kidney obtained at 30 min after injection of **5a** were examined with autoradiography and light microscopy after fixation and staining. The resulting autoradiographic images (Fig. 6) revealed that **5a** was mainly concentrated in the outer stripe of the outer medulla. This kidney region

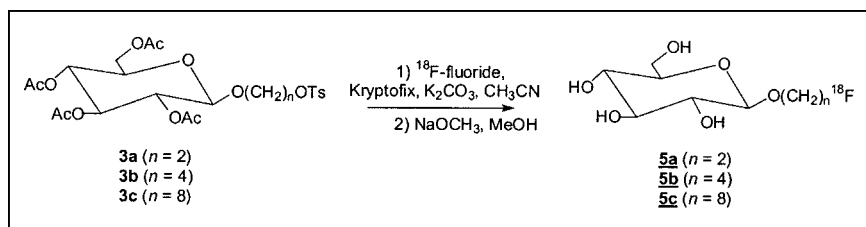


FIGURE 2. Synthesis of 2'- ^{18}F -fluoroethyl- β -D-glucoside (**5a**), ω - ^{18}F -fluoro-*n*-butyl- β -D-glucoside (**5b**), and ω - ^{18}F -fluoro-*n*-octyl- β -D-glucoside (**5c**).

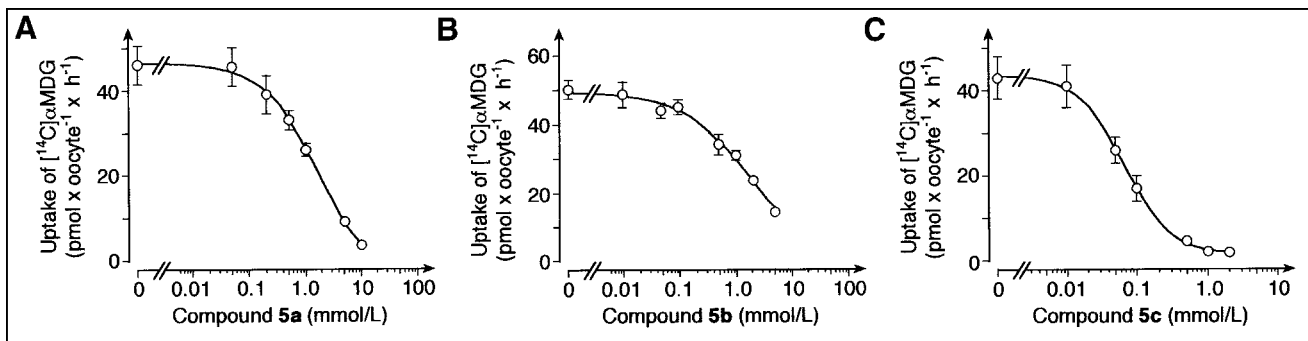


FIGURE 3. Inhibition of hSGLT1-expressed α MDG uptake by compounds **5a**, **5b**, and **5c**. *Xenopus* oocytes expressing hSGLT1 were incubated for 1 h with Ori buffer with or without 100 μ mol/L phlorizin plus 10 μ mol/L 14 C- α MDG and indicated concentrations of compound **5a**, **5b**, or **5c**. Mean values \pm SD of phlorizin-inhibited uptake rates measured from pairs of 7–10 oocytes are presented. Michaelis–Menten equation was fitted to data.

contains the S3 segments of the proximal tubules where SGLT1 is expressed (2).

Pretreatment of the mice with phlorizin 2 h before injection of **5a** showed a marked increase of urinary excretion. Phlorizin has a >100-fold higher affinity compared with D-glucose (24) and will partially block SGLT1 transport resulting in glucosuria. The observed increased urinary excretion of **5a** and the decreased retention in kidney (Table 1) indicate that tubular reabsorption of **5a** is indeed achieved by SGLT1.

HPLC analysis of plasma and urine samples collected at 30 min after injection of **5a** or **5b** revealed that >90% of the radioactivity in plasma and urine was in the form of intact tracer (Table 2). After injection of ω - 18 F-fluoro-*n*-octyl- β -D-glucoside (**5c**), only 38% was recovered in plasma as unchanged tracer, and in urine 72% of the radioactivity was present as unchanged tracer. The remainder of the radioactivity was found to be in the form of a more polar metabolite.

At 30 min after injection, only $19\% \pm 4\%$ ($n = 4$) of **5a** in the blood was detected in red blood cells. This was significantly lower than the fractions of **5b** ($38\% \pm 6\%$, $n = 2$, $P < 0.02$) and **5c** ($47\% \pm 3\%$, $n = 2$, $P < 0.002$) after this time period. This may be due to a higher passive diffusion of **5b** and **5c** compared with **5a** and suggests that

5a is not transported by GLUT1 that is expressed in erythrocytes (1).

DISCUSSION

The *in vitro* experiments in *Xenopus* oocytes showed that **5b** and **5c** were not transported by hSGLT1 but inhibited transport of α MDG. In contrast, **5a** was transported almost as efficiently as α MDG by hSGLT1. The *in vivo* experiments in mice, however, showed that an appreciable fraction of the injected dose of **5a** was excreted with the urine, whereas 14 C- α MDG revealed only a negligible urinary excretion (23). These apparent discordant results between *in vitro* and *in vivo* results may be caused by a different transport rate of **5a** by hSGLT1 versus mouse SGLT1 or by a different transport rate of **5a** and 14 C- α MDG by SGLT2. SGLT2 is a low-affinity, high-capacity transporter located in the S1 and S2 segments of the proximal tubules, whereas SGLT1 is a high-affinity, low-capacity transporter located in the S3 segment of the proximal tubules (2). The maximal transport rates of hSGLT1 for D-glucose, α MDG, and **5a** are similar (see above) (23). In human and mouse, α MDG may

FIGURE 4. Test whether compounds **5a**, **5b**, and **5c** are transported substrates of hSGLT1. *Xenopus* oocytes expressing hSGLT1 were clamped at -50 mV and superfused with sugar-free Ori buffer or with Ori buffer containing 5 mmol/L of α MDG, **5a**, **5b**, or **5c**. (A) Typical experiment with 1 oocyte. (B) Mean \pm SD values from 4 oocytes are presented.

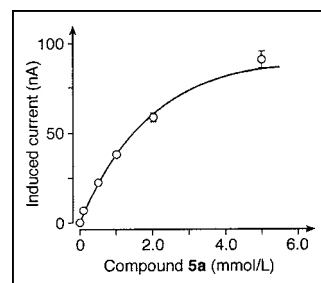
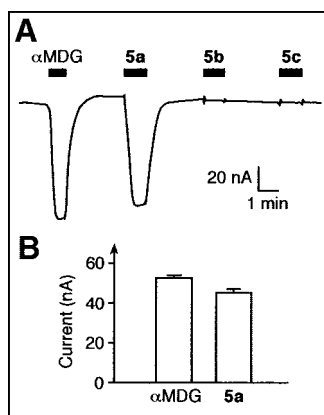


FIGURE 5. Substrate dependence of hSGLT1-expressed inward currents that are induced by compound **5a**. hSGLT1-expressing *Xenopus* oocytes clamped at -50 mV were superfused with Ori buffer containing indicated concentrations of **5a**, and currents induced by **5a** were measured. Mean \pm SD values from 4 oocytes are presented. Michaelis–Menten equation was fitted to data.

TABLE 1

Tissue Distribution in Mice of 2'-¹⁸F-Fluoroethyl-(**5a**), ω-¹⁸F-Fluorobutyl-(**5b**), and ω-¹⁸F-Fluorooctyl-β-D-Glucoside (**5c**)

Distribution	% Injected dose (n = 5; mean ± SD)						
	5a			5b		5c	
	10 min	30 min	30 min*	10 min	30 min	10 min	30 min
Bladder	5.2 ± 6.5	10.8 ± 6.0	53.8 ± 14.5	32.6 ± 8.5	51.0 ± 9.9	18.7 ± 14.5	43.3 ± 7.4
Kidneys	24.8 ± 4.8	22.3 ± 0.9	3.3 ± 1.6	21.0 ± 8.9	11.6 ± 3.7	11.6 ± 8.3	3.8 ± 2.1
Liver	8.0 ± 1.0	8.2 ± 0.7	3.8 ± 1.7	3.3 ± 0.3	2.3 ± 0.5	7.3 ± 1.4	3.9 ± 0.7
Spleen	0.7 ± 0.3	0.3 ± 0.1	0.2 ± 0.0	0.4 ± 0.1	0.4 ± 0.1	0.5 ± 0.2	0.3 ± 0.1
Lungs	1.2 ± 0.3	1.1 ± 0.2	0.5 ± 0.2	0.9 ± 0.2	0.6 ± 0.2	1.2 ± 0.3	0.5 ± 0.1
Heart	0.4 ± 0.1	0.3 ± 0.1	0.2 ± 0.1	0.3 ± 0.0	0.2 ± 0.1	0.5 ± 0.1	0.3 ± 0.1
Intestines	5.2 ± 0.4	4.5 ± 0.4	3.0 ± 1.8	3.2 ± 0.4	2.4 ± 0.6	6.9 ± 1.0	5.1 ± 0.7
Stomach	0.6 ± 0.1	0.7 ± 0.1	0.4 ± 0.2	0.5 ± 0.0	0.4 ± 0.1	0.7 ± 0.2	0.4 ± 0.1
Cerebrum	0.1 ± 0.0	0.1 ± 0.0	0.0 ± 0.0	0.0 ± 0.0	0.0 ± 0.0	0.2 ± 0.0	0.3 ± 0.0
Cerebellum	0.0 ± 0.0	0.0 ± 0.0	0.0 ± 0.0	0.0 ± 0.0	0.0 ± 0.0	0.1 ± 0.0	0.1 ± 0.0
Blood	13.8 ± 1.7	13.8 ± 1.6	6.0 ± 1.8	8.4 ± 1.0	5.3 ± 2.2	11.6 ± 1.2	5.2 ± 0.9
Carcass	49.1 ± 6.8	45.7 ± 4.7	27.6 ± 10.0	31.2 ± 2.3	26.0 ± 5.0	47.3 ± 5.9	39.5 ± 4.9

* Intraperitoneal pretreatment with 800 mg/kg body mass phlorizin, 2 h before tracer injection.

be a good substrate for both SGLT1 and SGLT2 and it may be removed almost completely from the glomerular filtrate during its passage through the S1 and S2 segments. If **5a** has a lower affinity for SGLT2, it will pass through the S1 and S2 segments and then will be reabsorbed by SGLT1 in the S3 segment. The low capacity of the SGLT1 transporter may not be sufficient to clear **5a** completely from the

glomerular filtrate, resulting in a partial urinary excretion. Glucoside **5a** may leave the proximal tubular cells only slowly, as it is probably a poor substrate for the GLUT2 transporter in the basolateral membrane. This would explain the transiently higher concentration in kidney at 30 min of **5a** compared with **5b** and **5c** and the slower decrease of concentration of **5a** in the blood.

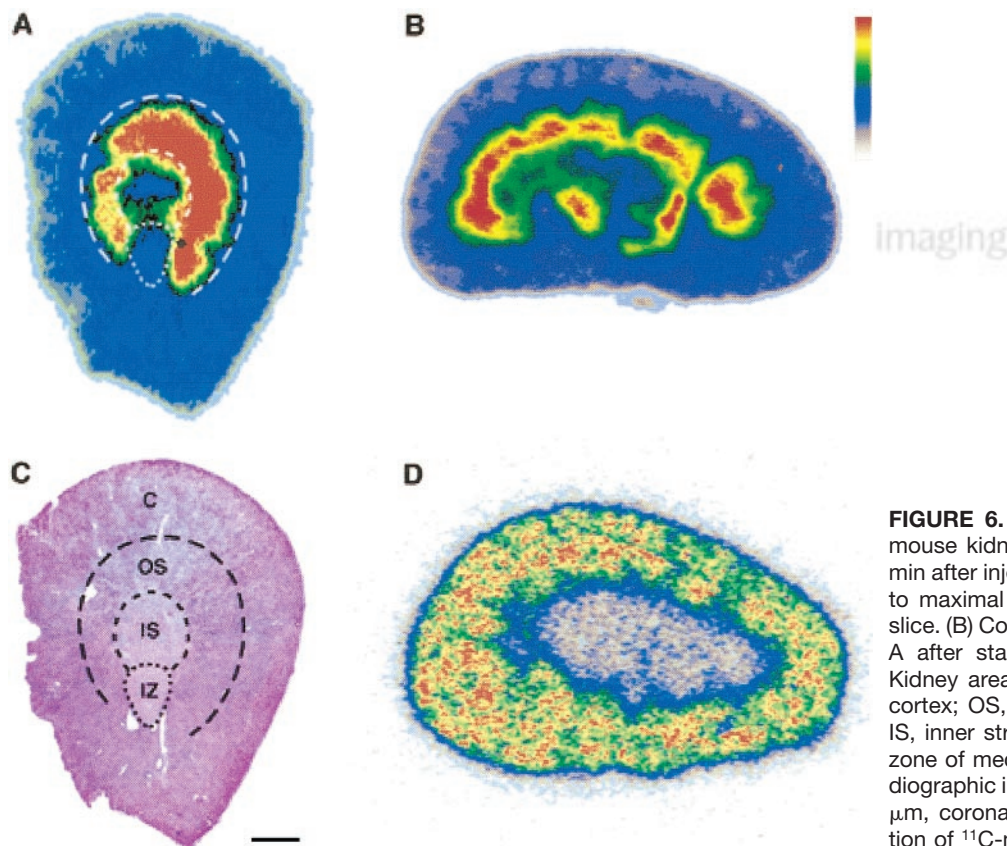


FIGURE 6. Autoradiographic images of mouse kidney slices (10 μm) obtained 30 min after injection of **5a**. Images are scaled to maximal pixel intensity. (A) Transverse slice. (B) Coronal slice. (C) Same section as A after staining with hematoxylin-eosin. Kidney areas are indicated as follows: C, cortex; OS, outer stripe of outer medulla; IS, inner stripe of outer medulla; IZ, inner zone of medulla. Bar = 1 mm. (D) Autoradiographic image of mouse kidney slice (25 μm, coronal) obtained 30 min after injection of ¹¹C-methyl-α-D-glucoside (**23**).

TABLE 2

Fraction of Unchanged Tracer in Plasma and Urine at 30 min After Intravenous Injection in Mice of 2'-¹⁸F-Fluoroethyl-(**5a**), ω-¹⁸F-Fluorobutyl-(**5b**), and ω-¹⁸F-Fluorooctyl-β-D-Glucoside (**5c**)

Compound	% in plasma*	% Intact tracer	
		Plasma†	Urine‡
5a	81 ± 4 (n = 4)	97 ± 1 (n = 5)	93 ± 1 (n = 3)
5b	63 ± 6 (n = 2)	92 ± 2 (n = 4)	94 ± 3 (n = 3)
5c	53 ± 3 (n = 2)	38 ± 6 (n = 5)	72 ± 7 (n = 4)

*Relative to total radioactivity in blood.
†Relative to total radioactivity in plasma.
‡Relative to total radioactivity in urine.
Data are mean ± SD.

The autoradiographic images of the intrarenal distribution (Figs. 6A and 6C) are consistent with these hypotheses. Glucoside **5a** was accumulated mainly in the outer part of the outer medulla. This kidney region, termed the "outer stripe," contains the S3 segments of renal proximal tubules where SGLT1 is expressed (2). The "inner stripe" contains no proximal tubules but pars rectae of distal tubules and vascular bundles with descending and ascending vasa rectae. At variance with the distribution of **5a**, ¹¹C-αMDG was mainly accumulated in the renal cortex that contains S1 and S2 segments of renal proximal tubules (23). No accumulation of ¹¹C-αMDG was observed in the outer stripe of the outer medulla because most ¹¹C-αMDG was cleared from the glomerular filtrate in the S1 and S2 segments (Fig. 6D).

The uptake of **5a** in kidney was also evaluated after pretreatment with phlorizin. Phlorizin is an inhibitor of SGLT1 and SGLT2 and its application leads to glucosuria. In our experiment, the pretreatment resulted in a reduced retention of **5a** in the kidneys and an increased excretion into the urine. The blood level was also markedly reduced. This is proof of the involvement of SGLT1 or SGLT2 in the accumulation of **5a** in the kidneys. Taken together, the data suggest that the activity of SGLT1 in humans can be visualized by **5a**, whereas the activity of both SGLT1 and SGLT2 can be visualized by ¹¹C-methyl-α-D-glucoside (23).

During acute renal failure, the S3 segments of proximal tubules and the thick ascending limbs of Henle are primarily and most strongly damaged (25). Since compound **5a** appears to be a selective marker for functional activity of SGLT1 and SGLT1 is expressed in the S3 segment, PET with compound **5a** may be used to detect early renal defects during acute renal failure.

In brain, the concentrations of **5a** and **5b** were very low and only a small fraction of **5c** was detected. The latter may be due to passive diffusion of the lipophilic compound through the plasma membranes of the BBB. The low uptake in brain suggests that **5a**, **5b**, and **5c** are not transported by GLUT1 that is expressed in the BBB (15,16). Recently we were able to immunolocalize SGLT1 in luminal membranes

of rat brain capillaries, suggesting that SGLT1 plays a role in the migration of D-glucose across the BBB (H. Koepsell, unpublished data, 2003). However, the concentration of SGLT1 in the brain is lower than that in the kidney and, until now, it is not clear whether SGLT1 expressed in brain is functional in normal physiologic conditions. This may explain the observed absence of accumulation of **5a** in brain.

CONCLUSION

Three ¹⁸F-labeled ligands—that is, 2'-¹⁸F-fluoroethyl-β-D-glucoside (**5a**), ω-¹⁸F-fluoro-*n*-butyl-β-D-glucoside (**5b**), and ω-¹⁸F-fluoro-*n*-octyl-β-D-glucoside (**5c**) were prepared and evaluated in an in vitro and in vivo model.

In vitro, **5a** was transported almost as efficiently as αMDG by SGLT1, whereas **5b** and **5c** were not transported but inhibited transport of αMDG. In vivo, **5a**, **5b**, and **5c** were cleared mainly by the kidneys, and **5a** was retained in the outer medulla of the kidney. The accumulation of **5a** could be blocked by pretreatment with phlorizin. Brain uptake of **5a** and **5b** was low, whereas **5c** showed limited brain uptake. The data indicate that **5a** appears to be a valid tracer for the specific in vivo visualization of SGLT1 activity. The accumulation of **5a** in the kidney may be used to visualize the outer stripe of the inner medulla with intact proximal tubules containing functional sodium/D-glucose cotransporter 1.

ACKNOWLEDGMENT

This research was supported by the National Fund for Scientific Research-Flanders, Belgium, and by the Deutsche Forschungsgemeinschaft (SFB 487/C1).

REFERENCES

- Wood IS, Trayhurn P. Glucose transporters (GLUT and SGLT): expanded families of sugar transport proteins. *Br J Nutr.* 2003;89:3-9.
- Hediger MA, Rhoads DB. Molecular physiology of sodium-glucose cotransporters. *Physiol Rev.* 1994;74:993-1025.
- Diez-Sampedro A, Lostao MP, Wright EM, Hirayama BA. Glycoside binding and translocation in Na⁺-dependent glucose cotransporters: comparison of SGLT1 and SGLT3. *J Membr Biol.* 2000;176:111-117.
- Mackenzie B, Panayotova-Heiermann M, Loo DDF, Lever JE, Wright EM. SAAT1 is a low affinity Na⁺/glucose cotransporter and not an amino acid transporter. *J Biol Chem.* 1994;269:22488-22491.
- Diez-Sampedro A, Hirayama BA, Osswald C, et al. A glucose sensor hiding in a family of transporters. *Proc Natl Acad Sci USA.* 2003;100:11753-11758.
- Veyhl M, Wagner K, Volk C, et al. Transport of the new chemotherapeutic β-D-glucosylisophosphoramidate mustard (D-195765) into tumor cells is mediated by the Na⁺-D-glucose cotransporter SAAT1. *Proc Natl Acad Sci USA.* 1998;95:2914-2919.
- Ishikawa N, Oguri T, Isobe T, Fujitaka K, Kohno N. SGLT gene expression in primary lung cancers and their metastatic lesions. *Jpn J Cancer Res.* 2001;92:874-879.
- Martin MG, Lostao MP, Turk E, Lam J, Kreman M, Wright EM. Compound missense mutations in the sodium/D-glucose cotransporter result in trafficking defects. *Gastroenterology.* 1997;112:1206-1212.
- Scriver SR, Chesney RW, McInnes RR. Genetic aspects of renal tubular transport: diversity and topology of carriers. *Kidney Int.* 1976;9:149-171.
- Pearson PY, Yu DH, Schwartz MZ. Transfection of the sodium/glucose cotransporter into colon mucosa: a novel treatment for short bowel syndrome. *J Pediatr Surg.* 2002;37:1076-1079.
- Tsujihara K, Hongu M, Saito K, et al. Na⁺-glucose cotransporter (SGLT) inhib-

- itors as antidiabetic agents. 4. Synthesis and pharmacological properties of 4'-dehydroxyphlorizin derivatives substituted on the B ring. *J Med Chem.* 1999; 42:5311–5324.
12. Boogaard PJ, Mulder GJ, Nagelkerke JF. Isolated proximal tubular cells from rat kidney as an in vitro model for studies on nephrotoxicity. II. α -Methylglucoside uptake as a sensitive parameter for mechanistic studies of acute toxicity by xenobiotics. *Toxicol Appl Pharmacol.* 1989;101:144–157.
 13. Poppe R, Karbach U, Gambaryan S, et al. Expression of the Na^+ -D-glucose cotransporter SGLT1 in neurons. *J Neurochem.* 1997;69:84–94.
 14. Nishizaki T, Matsuoka T. Low glucose enhances Na^+ /glucose transport in bovine brain artery endothelial cells. *Stroke.* 1998;29:844–849.
 15. Bell GI, Burant CF, Takeda J, Gould GW. Structure and function of mammalian sugar transporters. *J Biol Chem.* 1993;268:19161–19164.
 16. Nagamatsu S, Kornhauser JM, Burant CF, Seino S, Mayo KE, Bell GI. Glucose transporter expression in brain. *J Biol Chem.* 1992;267:467–472.
 17. Warfield AS, Segal S. Uptake of α -methyl-D-glucoside by synaptosomes from rat brain. *J Neurochem.* 1976;26:1275–1278.
 18. Ullrich KJ, Rumrich G, Klöss S. Specificity and sodium dependence of the active sugar transport in the proximal convolution of the rat kidney. *Pflügers Arch.* 1974;351:35–48.
 19. Kipp H, Lin JT, Kinne RKH. Interactions of alkylglucosides with the renal sodium/D-glucose cotransporter. *Biochim Biophys Acta.* 1996;1282:124–130.
 20. Dahmén J, Frejd T, Gronberg G, Lavet T, Magnusson G, Noori G. 2-Bromoethyl glycosides: synthesis and characterization. *Carbohydr Res.* 1983;116:303–307.
 21. Wallace JE, Schroeder LR. Koenigs-Knorr reactions. Part 1. Effects of a 2-acetyl substituent, the promotor, and the alcohol concentration on the stereoselectivity of reactions of 1,2-cis-glucopyranosyl bromide. *J Chem Soc [Perkin I].* 1976; 1938–1941.
 22. Furness BS, Hannaford AJ, Smith PW, Tatchell AR, eds. *Vogel's Textbook of Practical Organic Chemistry.* 5th ed. Essex, U.K.: Longman Scientific & Technical, 1989:649.
 23. Bormans GM, Van Oosterwyck G, de Groot TJ, et al. Synthesis and biologic evaluation of ^{11}C -methyl-D-glucoside, a tracer of the sodium dependent glucose transporter. *J Nucl Med.* 2003;44:1075–1081.
 24. Koepsell H, Fritsch G, Korn K, Madrala A. Two substrate sites in the renal Na^+ -D-glucose cotransporter studied by model analysis of phlorizin binding and D-glucose transport measurements. *J Membr Biol.* 1990;114:113–132.
 25. Bonventre JV, Brezis M, Siegel N, et al. Acute renal failure. I. Relative importance of proximal vs. distal tubular injury. *Am J Physiol Renal Physiol.* 1998; 275:F623–F631.

